arXiv:1212.1127v1 [hep-ph] 5 Dec 2012

Head shock vs Mach cone: azimuthal correlations from 2→3 parton processes in relativistic heavy-ion collisions

Alejandro Ayala[1], Isabel Dominguez[1] and Maria Elena Tejeda-Yeomans[2]
[1] *Instituto de Ciencias Nucleares, Universidad Nacional Autónoma de México, Apartado Postal 70-543, México Distrito Federal 04510, Mexico.*
[2] *Departamento de Física, Universidad de Sonora, Boulevard Luis Encinas J. y Rosales, Colonia Centro, Hermosillo, Sonora 83000, Mexico.*

We study the energy-momentum deposited by fast moving partons within a medium using linearized viscous hydrodynamics. The particle distribution produced by this energy-momentum is computed using the Cooper-Frye formalism. We show that for the conditions arising in heavy-ion collisions, energy momentum is preferentially deposited along the head shock of the fast moving partons. We also show that the double hump in the away-side of azimuthal correlations can be produced by two (instead of one) away-side partons that deposit their energy-momentum along their directions of motion. These partons are originated in the in-medium hard scattering in $2 \rightarrow 3$ processes. We compare the results of the analysis to azimuthal angular correlations from PHENIX and show that the calculation reproduces the data systematics of a decreasing away-side correlation when the momentum of the associated hadron becomes closer to the momentum of the leading hadron. This scenario seems to avoid the shortcomings of the Mach cone as the origin of the double-hump structure in the away-side.

PACS numbers: 25.75.-q, 25.75.Gz, 24.10.Lx, 24.10.Nz

I. INTRODUCTION

Azimuthal angular correlations have provided a powerful testing ground to elucidate the propagation properties of fast partons within the medium created in high-energy heavy-ion reactions [1, 2]. The main features of these correlations can be summarized as follows: when the leading and the the away-side particles have similar momenta, the correlation shows a suppression of the away-side peak, compared to proton collisions at the same energies. However, when the momentum difference between leading and away-side particles increases, either a double peak or a broadening of the away-side peak appears, while neither of these are present in proton collisions at the same energies [3]. The peak region is known as the shoulder and the region between the peaks is known as the head. For low momentum particles, the jet multiplicity is larger in the shoulder than in the head region [2].

Since the structures in the away-side are best seen for low momentum particles, there were explanations based on the emission of sound modes caused by one fast moving parton [4, 5], the so called *Mach cones*. Nevertheless, it has been argued that such interpretation is fragile, since the jet-medium interaction produces also a wake whose contribution cannot be ignored [6, 7]. Furthermore, it has recently been shown that it is unlikely that the propagation of one high energetic particle through the medium leads to a double peak structure in the azimuthal correlation in a system of the size and finite viscosity relevant for heavy ion collisions, since the energy-momentum deposition in the head shock region is strongly forward-peaked [8]. Moreover, by using a realistic multiple gluon emission for the parton shower produced by an in-medium moving parton, the overlapping perturbations in very different spatial directions wipe out any distinct Mach cone structure [9].

The more widely accepted explanation for the double peak/broadening of the away-side is given nowadays in terms of initial state fluctuations of the matter density in the colliding nuclei. These fluctuations are then shown to give rise to an anisotropic flow of partially equilibrated, low momentum particles, within the bulk medium. Hydrodynamic descriptions of this scenario have for instance successfully reproduced the experimental v_3 [10]. However, it has also been shown that there is a strong connection between the observed away-side structures and the medium's path length [11]. The connection is expressed through the dependence of the azimuthal correlation on the trigger particle direction with respect to the event plane in such a way that, for selected trigger and associated particle momenta, the double peak is present/absent for out of plane/in plane trigger particle direction. A final state effect rather than an an initial state one seems more consistent with this observation.

The medium's response to a fast moving parton can be described by the energy and momentum that the parton deposits. This energy-momentum is then converted into particles upon hadronization. When the interaction produces low momentum particles, a hydrodynamical description of the medium's response seems appropriate. In this framework, it is natural to explore the types of medium excitations generated by fast moving partons and the way these in turn are responsible for the shape of the away-side in the angular correlations. When the *sound* (that is the *longitudinal modes*) are prominently excited, the double peak in the away-side could emerge as a Mach cone structure, that is, as energy-momentum mainly deposited on the sides of the path travelled by the parton. This is illustrated in the left panel of fig. 1. However, when the modes that get prominently excited

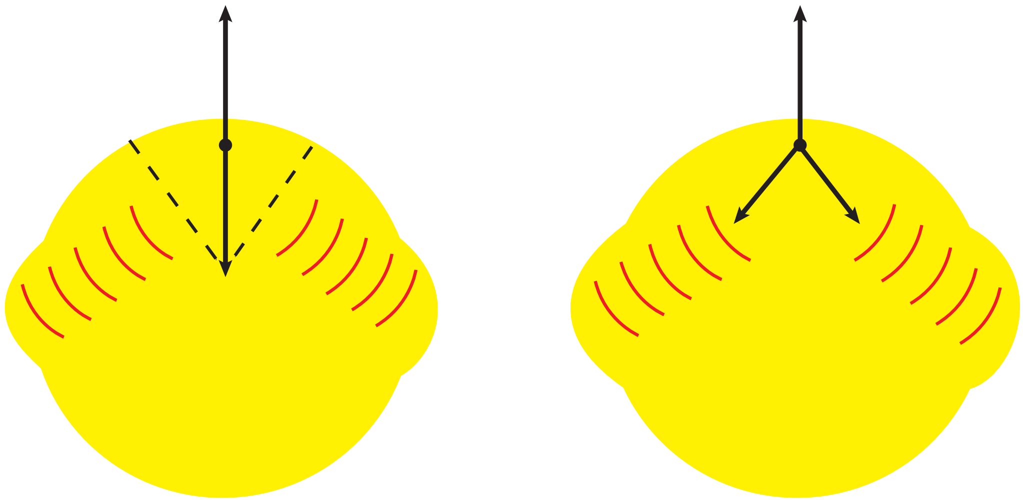

FIG. 1: (Color on-line) Schematic representation of the possible origin of the away-side double-hump. The left panel illustrates the common picture whereby one away-side parton deposits energy-momentum, exciting the sound modes and producing a Mach cone. The right panel illustrates our approach whereby two away-side partons generate each a head-shock and deposit energy-momentum preferentially along their directions of motion.

are the *wake*, (that is the *transverse modes*), energy and momentum is preferentially deposited along the direction of the travelling parton. If a double peak is to emerge, the alternative scenario is that the structure is produced by two travelling partons in the away-side. This is illustrated in the right panel of fig. 1.

Two partons in the away-side are produced in processes where two initial state partons scatter into three final state ones, the so called 2 → 3 processes. In this case the cross section is smaller than the one for 2 → 2 processes, at least by one power of α_s. However, consider a scattering event that deposits a given amount of energy in the away-side. If such event comes from a 2 → 2 process, the away-side parton will have a larger energy than each of the two partons, when these last come from a 2 → 3 process. Since the parton distribution is a fast falling function of the parton energy, the extra power of α_s is partially compensated by the larger abundance of partons with smaller energy. This is illustrated in fig. 2. For 2 → 3 processes, when the dominant energy-momentum deposition happens through transverse modes, conservation of momentum at the parton level gives rise to a distinctive angular dependence in the azimuthal correlation whereby, the angular difference between the peaks in the away-side is close to $2\pi/3$ radians.

The computation of hadron events produced by 2 → 3 parton processes in the context of azimuthal correlation functions has been put forward and explored in Refs. [12, 13], using the leading order QCD matrix elements. Those studies were made for fragmentation outside the medium. In this work we compute the hadron multiplicity produced by two partons in the away-side coming from 2 → 3 processes for the case where all its energy-momentum is deposited into the medium. We use linearized viscous hydrodynamics to compute the medium's response. The work is organized as follows: In Sec. II we first review the general framework to compute the particle distribution stemming from a given energy-momentum deposited by a fast moving parton within the medium, using linearized viscous hydrodynamics. This energy-momentum is then converted into a parton multiplicity using the Cooper-Frye formalism [14]. We discuss the different shapes for the azimuthal correlations that

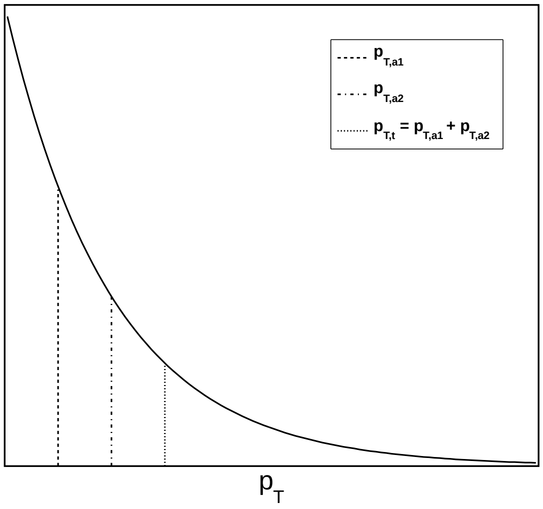

FIG. 2: Schematic representation of how a single away-side parton is less abundantly produced than two away-side partons carrying the same total momentum, given that the momentum distribution function rapidly decays with momentum.

are obtained when varying the strength of the wake and sound mode contributions. In Sec. III we solve the hydrodynamic equations for the transverse and longitudinal modes. We work in the limit where the patron's velocity is larger than the sound velocity. In Sec. IV we use these solutions to compute the azimuthal correlations by convoluting the pQCD probability to produce two away-side partons in $2 \to 3$ processes with the multiplicity obtained from the excess of energy-momentum produced by the moving partons followed by fragmentation. We finally summarize and conclude in Sec. V.

II. PARTICLE DISTRIBUTION

We compute the particle's multiplicity as given by the Cooper-Frye formula

$$E\frac{dN}{d^3p} = \frac{1}{(2\pi)^3}\int d\Sigma_\mu p^\mu [f(p\cdot u) - f(p_0)], \tag{1}$$

where $f(p\cdot u) - f(p_0)$ is the phase-space disturbance produced by the fast moving parton on top of the equilibrium distribution $f(p_0)$, with Σ_μ and p_μ representing the freeze-out hyper-surface and the particle's momentum, respectively. The medium's total four-velocity $u^\mu \equiv u_0^\mu + \delta u^\mu$ is made out of two parts: the background four-velocity u_0^μ and the disturbance δu^μ. This last contribution is produced by the fast moving parton and can be computed using viscous linear hydrodynamics once the source, representing the parton, is specified. For a static background (which hereby we assume) and in the linear approximation, u^μ can be written as

$$\begin{aligned} u^\mu &\equiv u_0^\mu + \delta u^\mu \\ &= \left(1, \frac{\mathbf{g}}{\epsilon_0(1+c_s^2)}\right), \end{aligned} \tag{2}$$

where the spatial part of the medium's four-velocity, $\mathbf{u} = \mathbf{g}/\epsilon_0(1+c_s^2)$, is written for convenience in terms of the momentum density $\mathbf{g}$ associated to the disturbance, with ϵ_0 and c_s the static background's energy density and sound velocity, respectively. We focus on events at central rapidity, $y \simeq 0$ and take the direction of motion of the fast parton to be the $\hat{z}$ axis and the beam axis to be the $\hat{x}$ axis. With this geometry, the transverse plane is the $\hat{y} - \hat{z}$ plane and therefore, the momentum four-vector for a (massless) particle is explicitly given by

$$\begin{aligned} p_\mu &= (E, p_x, p_y, p_z) \\ &= (p_T, 0, p_T\sin\phi, p_T\cos\phi), \end{aligned} \tag{3}$$

where ϕ is the angle that the momentum vector $\mathbf{p}$ makes with the $\hat{z}$ axis. We use Bjorken's geometry, thus

$$\begin{aligned} d^3p &= p_T dp_T d\phi dp_x \\ p_x &= p_T \sinh y \\ dp_x &= p_T \cosh y\ dy \\ E &= p_T \cosh y, \end{aligned} \tag{4}$$

and therefore

$$E\frac{dN}{d^3p} = \frac{1}{p_T dp_T}\frac{dN}{d\phi dy}. \tag{5}$$

For simplicity we consider a freeze-out hyper-surface of constant time

$$d\Sigma_\mu = (d^3r, 0, 0, 0). \tag{6}$$

Therefore, using Eqs. (1) and (5), the particle azimuthal distribution around the direction of motion of a fast moving parton within the p_T interval $p_T^{\text{min}} \leq p_T \leq p_T^{\text{miax}}$ is given by

$$\begin{aligned} \left.\frac{dN}{dy}\right|_{y\simeq 0} &= \frac{\Delta\tau\Delta y}{(2\pi)^3}\int_{p_T^{\text{min}}}^{p_T^{\text{max}}} dp_T p_T^2 \\ &\times \int d^2r [f(p\cdot u) - f(p_0)], \end{aligned} \tag{7}$$

with $\Delta\tau$ the freeze-out time interval and where we have assumed perfect correlation between the space-time rapidity η and y to substitute $\Delta\eta$ by Δy. We assume that the equilibrium distribution is of the Boltzmann type. In this way, we have

$$\begin{aligned} f(p_0) &= \exp[p_T/T_0] \\ f(p\cdot u) &= \exp\left[\frac{p_T}{(T_0+\delta T)}\left(1 - \frac{\mathbf{g}_y\sin\phi + \mathbf{g}_z\cos\phi}{\epsilon_0(1+c_s^2)}\right)\right], \end{aligned} \tag{8}$$

where T_0 is the background medium's temperature and δT is the change in temperature caused by the passing of the fast parton. Assuming that the energy density and temperature are related through Boltzmann's law

$$\epsilon \propto T^4, \tag{9}$$

one gets

$$\frac{\delta T}{T_0} = \frac{\delta\epsilon}{4\epsilon_0}. \tag{10}$$

Since for the validity of linearized hydrodynamics, both $\delta\epsilon$ and $\mathbf{g}$ need to be small quantities compared to ϵ_0, we can expand the difference $f(p\cdot u) - f(p_0)$ to linear order. Using Eqs. (8) and (10) we get

$$\begin{aligned} f(p\cdot u) - f(p_0) &\simeq \left(\frac{p_T}{T_0}\right)\exp\left[-p_T/T_0\right] \\ &\times \left(\frac{\delta\epsilon}{4\epsilon_0} + \frac{\mathbf{g}_y\sin\phi + \mathbf{g}_z\cos\phi}{\epsilon_0(1+c_s^2)}\right), \end{aligned} \tag{11}$$

therefore the particle azimuthal distribution around the direction of motion of a fast moving parton is given, in the linear approximation, by

$$\begin{aligned} \left.\frac{dN}{dy}\right|_{y\simeq 0} &= \frac{\Delta\tau\Delta y}{(2\pi)^3}\int_{p_T^{\text{min}}}^{p_T^{\text{max}}} dp_T \frac{p_T^3}{T_0}\exp\left[-p_T/T_0\right] \\ &\times \int d^2r\left(\frac{\delta\epsilon}{4\epsilon_0} + \frac{\mathbf{g}_y\sin\phi + \mathbf{g}_z\cos\phi}{\epsilon_0(1+c_s^2)}\right). \end{aligned} \tag{12}$$

Notice that the shape of the distribution around the direction of the fast moving parton depends on the quantities

$$\begin{aligned} G_y &\equiv \int d^2r\mathbf{g}_y \\ G_z &\equiv \int d^2r\mathbf{g}_z. \end{aligned} \tag{13}$$

When $G_y > G_z$ the distribution is dominated by the $\sin\phi$ factor, giving rise to two peaks away from $\phi = 0$. However, when $G_z > G_y$ the opposite happens and the distribution is dominated by the $\cos\phi$ factor with the two peaks close to $\phi = 0$. These peaks become a single peak in the extreme case where $G_z \gg G_y$. This is illustrated in fig. 3.

We now proceed to show that when the velocity of the moving parton is larger than the speed of sound, G_y is mostly made out of longitudinal (sound) modes, whereas G_z is mostly made out of wake (transverse) modes and that the latter dominates the former, giving rise to a particle distribution centered around the direction of motion of the moving parton.

III. LINEAR VISCOUS HYDRODYNAMICS

In order to compute the g_y and g_z components of the momentum density vector $\mathbf{g}$ which is deposited into the medium by the moving fast parton, we resort to using linearized viscous hydrodynamics. Assuming that the disturbance introduced by the parton is small, the medium's energy-momentum tensor can be written as

$$\Theta^{\mu\nu} = \Theta_0^{\mu\nu} + \delta\Theta^{\mu\nu} \tag{14}$$

where $\delta\Theta^{\mu\nu}$ is the perturbation generated by the parton and $\Theta_0^{\mu\nu}$ is the equilibrium energy-momentum tensor of the underlying medium. Therefore each of these components satisfy the equations

$$\begin{aligned} \partial_\mu\delta\Theta^{\mu\nu} &= J^\nu \\ \partial_\mu\Theta_0^{\mu\nu} &= 0, \end{aligned} \tag{15}$$

where J^ν represents the source of the disturbance, which in this case corresponds to the fast moving parton. Here we consider that the parton can be represented by a localized disturbance of the form

$$J^\nu(\mathbf{x},t) = \left(\frac{dE}{dx}\right) v^\nu \delta(\mathbf{x} - \mathbf{v}t), \tag{16}$$

where (dE/dx) is the energy loss per unit length and

$$v^\nu = \gamma(1, \mathbf{v}), \tag{17}$$

with γ the Lorentz gamma factor. Effects of a finite source structure have been studied in Ref. [15] where it is found that differences in the energy density deposition between a finite extent source and a localized one

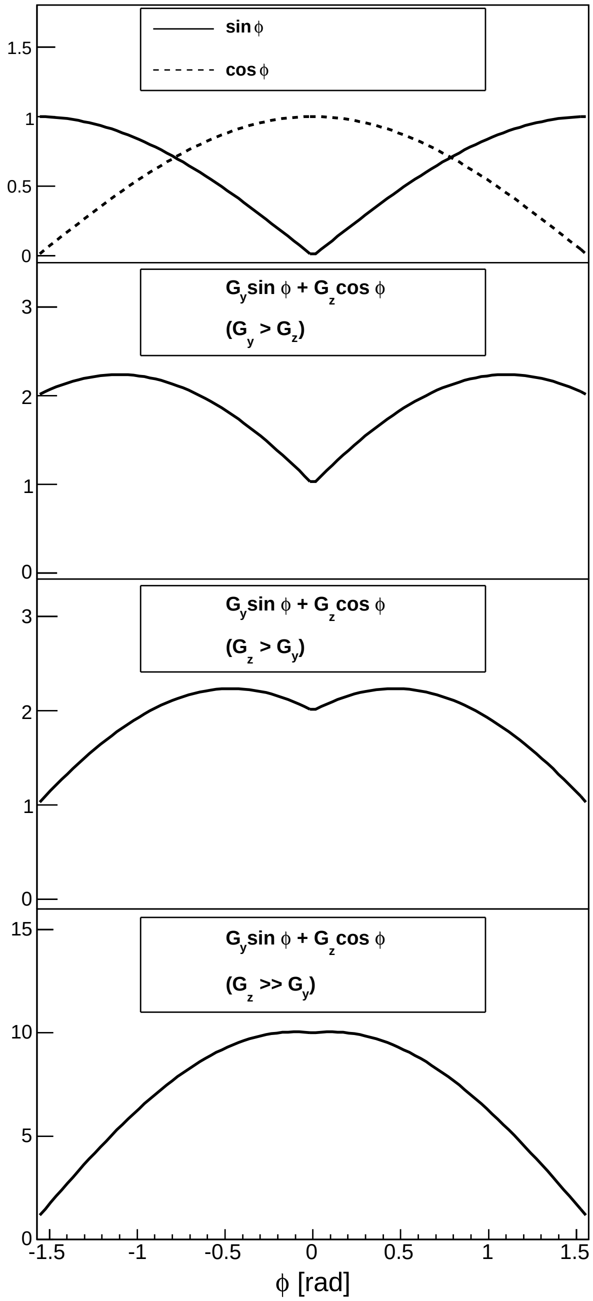

FIG. 3: Schematic representation of the particle distribution, arising from the Cooper-Frye formula. The distribution is centered around the direction of motion ($\phi = 0$) of the parton that deposits the energy-momentum in the medium. Since the distribution is a sum of a $\sin(\phi)$ and a $\cos(\phi)$, its shape depends on the relative strength of their respective coefficients G_y and G_z. From top to bottom, we show first the $\sin(\phi)$ and a $\cos(\phi)$ functions, the case where $G_y > G_z$, the case where $G_z > G_y$ and finally the case where $G_z \gg G_y$.

exist only close to the source. Since a hydrodynamical description is anyway valid only for large distances from the source, compared to the transport mean free path, here we will consider that the description of a source as localized exactly at the position of the fast parton suffices.

To describe the propagation of the disturbance caused by the source, Eqs. (15) are solved by considering that the energy-momentum tensor $\Theta^{\mu\nu}$ consists of a piece that describes an isotropic fluid

$$\Theta_0^{\mu\nu} = -pg^{\mu\nu} + (\epsilon + p)u_0^\mu u_0^\nu \tag{18}$$

and a disturbance $\delta\Theta^{\mu\nu}$ caused by the source, whose explicit components to first order in shear (η) and bulk (ζ) viscosity, are given by

$$\begin{aligned}
\delta\Theta^{00} &= \delta\epsilon, \\
\delta\Theta^{0i} &= \mathbf{g}, \\
\delta\Theta^{ij} &= \delta_{ij}c_s^2\delta\epsilon - \frac{3}{4}\Gamma_s(\partial^i\mathbf{g}^j + \partial^j\mathbf{g}^i - \frac{2}{3}\delta_{ij}\nabla\cdot\mathbf{g}) \\
&- \zeta\,\delta_{ij}\nabla\cdot\mathbf{g},
\end{aligned} \tag{19}$$

where $\epsilon(t,\mathbf{x}) = \epsilon_0 + \delta\epsilon(t,\mathbf{x})$ with ϵ_0 corresponding to the energy density of the background fluid, $\delta\epsilon$ to the energy density associated to the disturbance and

$$\Gamma_s \equiv \frac{4\eta}{3\epsilon_0(1+c_s^2)} \tag{20}$$

is the sound attenuation length.

In the linear approximation and vanishing bulk viscosity [15], the dynamical description of the propagation of the disturbance is given by the first of Eqs. (15), whose explicit components can be written as

$$\begin{aligned}
\partial_0\delta\epsilon + \nabla\cdot\mathbf{g} &= J^0, \\
\partial_0\mathbf{g}^i + \partial_j\delta\Theta^{ij} &= J^i.
\end{aligned} \tag{21}$$

These equations can be readily solved in momentum space. We define the Fourier transform pair $f(\mathbf{x},t)$ and $f(\mathbf{k},\omega)$ as

$$f(\mathbf{x},t) = \frac{1}{(2\pi)^4}\int d^3k\int d\omega\, e^{i\mathbf{k}\cdot\mathbf{x}-i\omega t}f(\mathbf{k},\omega). \tag{22}$$

Using Eq. (22) into Eqs. (21), together with Eqs. (19), we obtain

$$\begin{aligned}
-i\omega\delta\epsilon + i\mathbf{k}\cdot\mathbf{g} &= J^0, \\
-i\omega\mathbf{g}^i + ic_s^2k^i\delta\epsilon + \frac{3}{4}\Gamma_s(k^2\mathbf{g}^i + \frac{k^i}{3}(\mathbf{k}\cdot\mathbf{g})) &= J^i.
\end{aligned} \tag{23}$$

Thus the perturbed energy density, $\delta\epsilon$ and momentum density components $\mathbf{g}^i$, can be obtained by solving the algebraic system of Eqs. (23) and the solutions are given by [16]

$$\delta\epsilon(\mathbf{k},\omega) = \frac{i\mathbf{k}\cdot\mathbf{J}(\mathbf{k},\omega) + J^0(\mathbf{k},\omega)(i\omega - \Gamma_sk^2)}{\omega^2 - c_s^2k^2 + i\Gamma_s\omega k^2}, \tag{24}$$

$$\mathbf{g}_L(\mathbf{k},\omega) = \frac{i\left[\frac{\omega}{k^2}\mathbf{k}\cdot\mathbf{J}(\mathbf{k},\omega) + c_s^2J^0(\mathbf{k},\omega)\right]\mathbf{k}}{\omega^2 - c_s^2k^2 + i\Gamma_s\omega k^2}, \tag{25}$$

$$\mathbf{g}_T(\mathbf{k},\omega) = \mathbf{g} - \mathbf{g}_L = \frac{i\mathbf{J}_T(\mathbf{k},\omega)}{\omega + i\frac{3}{4}\Gamma_sk^2}, \tag{26}$$

where we have written the momentum density vector in terms of its transverse and longitudinal components with respect to the Fourier mode $\mathbf{k}$, namely

$$\mathbf{g} = \mathbf{g}_L + \mathbf{g}_T \tag{27}$$

with the definition of longitudinal and transverse components of any vector $\boldsymbol{\sigma}$ given by

$$\begin{aligned}
\boldsymbol{\sigma}_L &\equiv \frac{(\boldsymbol{\sigma}\cdot\mathbf{k})}{k^2}\mathbf{k} \\
\boldsymbol{\sigma}_T &\equiv \boldsymbol{\sigma} - \boldsymbol{\sigma}_L.
\end{aligned} \tag{28}$$

Note that the source term J^ν in Eq. (16) is Fourier transformed to

$$J^\nu(\mathbf{k},\omega) = (2\pi)\gamma\left(\frac{dE}{dx}\right)\delta(\mathbf{k}\cdot\mathbf{v} - \omega)v^\nu, \tag{29}$$

where we have assumed a constant energy loss per unit length.

From Eqs. (24)–(26) one can obtain the space time solutions for $\delta\epsilon(\mathbf{x},t)$ and $\mathbf{g}(\mathbf{x},t)$ upon use of Eq. (22). The corresponding expressions are

$$\begin{aligned}
\mathbf{g}_T(\mathbf{x},t) &= i\gamma(2\pi)\left(\frac{dE}{dx}\right)\int\frac{d^3k}{(2\pi)^3}\int\frac{d\omega}{(2\pi)}e^{i\mathbf{k}\cdot\mathbf{x}-i\omega t} \\
&\times \left[\mathbf{v} - \frac{(\mathbf{k}\cdot\mathbf{J})\mathbf{k}}{k^2}\right]\frac{\delta(\mathbf{k}\cdot\mathbf{v}-\omega)}{\omega + i\frac{3}{4}\Gamma_sk^2}
\end{aligned} \tag{30}$$

$$\begin{aligned}
\mathbf{g}_L(\mathbf{x},t) &= i\gamma(2\pi)\left(\frac{dE}{dx}\right)\int\frac{d^3k}{(2\pi)^3}\int\frac{d\omega}{(2\pi)}e^{i\mathbf{k}\cdot\mathbf{x}-i\omega t} \\
&\times \mathbf{k}\left[\frac{\omega}{k^2}\mathbf{k}\cdot\mathbf{v} + c_s^2\right]\frac{\delta(\mathbf{k}\cdot\mathbf{v}-\omega)}{\omega^2 - c_s^2k^2 + i\Gamma_s\omega k^2}
\end{aligned} \tag{31}$$

and

$$\begin{aligned}
\delta\epsilon(\mathbf{x},t) &= i\gamma(2\pi)\left(\frac{dE}{dx}\right)\int\frac{d^3k}{(2\pi)^3}\int\frac{d\omega}{(2\pi)}e^{i\mathbf{k}\cdot\mathbf{x}-i\omega t} \\
&\times \left[i\mathbf{k}\cdot\mathbf{v} + i\omega - \Gamma_sk^2\right]\frac{\delta(\mathbf{k}\cdot\mathbf{v}-\omega)}{\omega^2 - c_s^2k^2 + i\Gamma_s\omega k^2}.
\end{aligned} \tag{32}$$

In order to compute the integrals in Eqs. (30)–(32) we use cylindrical coordinates with the k_z direction along the direction of motion $\mathbf{v}$ of the fast parton. It is easier to start with the components of $\mathbf{g}_T$. After carrying out the frequency and angular integration, we get for the z component

$$
\begin{aligned}
(\mathbf{g}_T)_z &= i\gamma(2\pi)\left(\frac{dE}{dx}\right)v\int_0^\infty\frac{dk_T}{(2\pi)^2}\int_{-\infty}^\infty\frac{dk_z}{(2\pi)}e^{ik_z(z-vt)} \\
&\times\frac{k_T^3\mathrm{J}_0(k_Tx_T)}{(k_z^2+k_T^2)[vk_z+i\frac{3}{4}\Gamma_s(k_z^2+k_T^2)]}, \qquad (33)
\end{aligned}
$$

where J_0 is a Bessel function and $x_T=\sqrt{y^2}$ is the distance from the parton along the transverse direction (along the $\hat{y}$ axis in the geometry we are using). The integration over k_z is performed using contour integration. For causal motion $(z-vt>0)$ we close the contour on the lower half k_z-plane. The poles that contribute are located at

$$
k_z=\left\{\begin{array}{c}-ik_T \\ i\frac{2v}{3\Gamma_s}\left(1-\sqrt{1+\left(\frac{3\Gamma_sk_T}{2v}\right)^2}\right)\end{array}\right. . \qquad (34)
$$

After carrying out the k_z integration, the remaining integral can be expressed in terms of the dimensionless quantities

$$
\begin{aligned}
\xi &\equiv \left(\frac{3\Gamma_s}{2v}\right)k_T \\
\alpha &\equiv |z-vt|/\left(\frac{3\Gamma_s}{2v}\right) \\
\beta &\equiv x_T/\left(\frac{3\Gamma_s}{2v}\right), \qquad (35)
\end{aligned}
$$

as

$$
\begin{aligned}
(\mathbf{g}_T)_z &= -\left(\frac{\gamma}{4\pi}\right)\left(\frac{dE}{dx}\right)\left(\frac{2v}{3\Gamma_s}\right)^2\int_0^\infty d\xi\ \xi\mathrm{J}_0(\xi\beta) \\
&\times\left[e^{-\alpha\xi}+\frac{e^{-\alpha(\sqrt{1+\xi^2}-1)}}{[\sqrt{1+\xi^2}-(1+\xi^2)]}\right]. \qquad (36)
\end{aligned}
$$

The first term in Eq. (36) can be analytically integrated. For numerical purposes, it is more convenient to rewrite the second term after the change of variable

$$
s=\sqrt{1+\xi^2}-1. \qquad (37)
$$

The final result is

$$
\begin{aligned}
(\mathbf{g}_T)_z &= \left(\frac{\gamma}{4\pi}\right)\left(\frac{dE}{dx}\right)\left(\frac{2v}{3\Gamma_s}\right)^2\left[-\frac{\alpha}{(\alpha^2+\beta^2)^{\frac{3}{2}}}\right. \\
&+\left.\int_0^\infty ds(s+2)\mathrm{J}_0\left(\beta\sqrt{s(s+2)}\right)e^{-\alpha s}\right] \\
&\equiv \left(\frac{\gamma}{4\pi}\right)\left(\frac{dE}{dx}\right)\left(\frac{2v}{3\Gamma_s}\right)^2 I_{g_{Tz}}(\alpha,\beta). \qquad (38)
\end{aligned}
$$

In a similar fashion we get

$$
\begin{aligned}
(\mathbf{g}_T)_y &= \left(\frac{\gamma}{4\pi}\right)\left(\frac{dE}{dx}\right)\left(\frac{2v}{3\Gamma_s}\right)^2\left[\frac{\beta}{(\alpha^2+\beta^2)^{\frac{3}{2}}}\right. \\
&-\left.\int_0^\infty ds\sqrt{s(s+2)}\mathrm{J}_1\left(\beta\sqrt{s(s+2)}\right)e^{-\alpha s}\right] \\
&\equiv \left(\frac{\gamma}{4\pi}\right)\left(\frac{dE}{dx}\right)\left(\frac{2v}{3\Gamma_s}\right)^2 I_{g_{Ty}}(\alpha,\beta). \qquad (39)
\end{aligned}
$$

The computation of the components of $\mathbf{g}_L$ is more involved due to the analytic structure of the poles in the complex k_z-plane. Let us fist compute the z component. After carrying out the frequency and angular integration we get

$$
\begin{aligned}
(\mathbf{g}_L)_z &= i\gamma(2\pi)\left(\frac{dE}{dx}\right)\int_0^\infty\frac{dk_T}{(2\pi)^2}\int_{-\infty}^\infty\frac{dk_z}{(2\pi)}e^{ik_z(z-vt)} \\
&\times\frac{k_T\mathrm{J}_0(k_Tx_T)k_z[k_z^2+\frac{c_s^2}{v^2}(k_z^2+k_T^2)]}{(k_z^2+k_T^2)[k_z^2+(i\frac{\Gamma_s}{v}k_z-\frac{c_s^2}{v^2})(k_z^2+k_T^2)]}. \qquad (40)
\end{aligned}
$$

Notice that the integrand contains the parameter c_s^2/v^2. For a fast moving (massless) parton $v\simeq 1$ and for a relativistic gas, $c_s\simeq\sqrt{1/3}$. Therefore, for conditions close to the ones after a heavy-ion reaction $c_s^2/v^2<1$ and we can expand the integrand in Eq. (40) in this parameter. To first order in c_s^2/v^2, we get

$$
\begin{aligned}
(\mathbf{g}_L)_z &= i\gamma(2\pi)\left(\frac{dE}{dx}\right)\int_0^\infty\frac{dk_T}{(2\pi)^2}k_T\mathrm{J}_0(k_Tx_T) \\
&\int_{-\infty}^\infty\frac{dk_z}{(2\pi)} \\
&\times\left\{\frac{k_z^2e^{ik_z(z-vt)}}{(k_z^2+k_T^2)[k_z+(i\frac{\Gamma_s}{v})(k_z^2+k_T^2)]}\right. \\
&+\left.\left(\frac{c_s^2}{v^2}\right)\frac{2k_z(i\frac{\Gamma_s}{v})(k_z^2+k_T^2)e^{ik_z(z-vt)}}{[k_z+(i\frac{\Gamma_s}{v})(k_z^2+k_T^2)]}\right\}. \\
&\qquad (41)
\end{aligned}
$$

For causal motion $(z-vt>0)$ we close the contour on the lower half k_z-plane. The poles that contribute are located at

$$
k_z=\left\{\begin{array}{c}-ik_T \\ i\frac{v}{2\Gamma_s}\left(1-\sqrt{1+\left(\frac{2\Gamma_sk_T}{v}\right)^2}\right)\end{array}\right. . \qquad (42)
$$

The remaining integral over k_T can be expressed in terms of the dimensionless quantities defined in Eq. (35). For numerical purposes, it is more convenient to rewrite this integral after the change of variable in Eq. (37). The

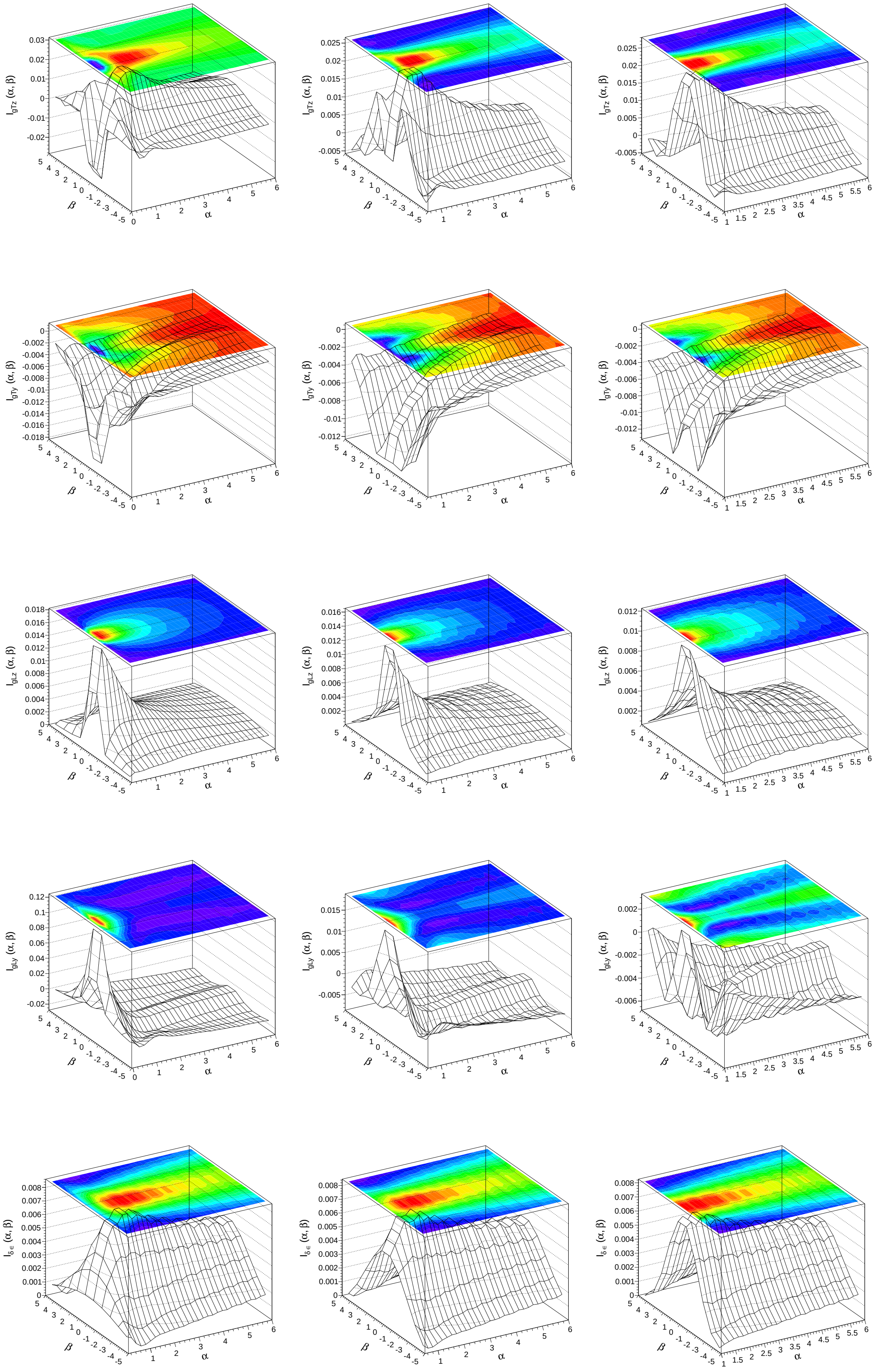

FIG. 4: (Color on-line) Three dimensional plots and the corresponding contour plots for (top to bottom) $I_{g_{Tz}}, I_{g_{Ty}}, I_{g_{Lz}}, I_{g_{Ly}}$ and $I_{g_{\delta\epsilon}}$ defined in Eqs. (38), (39), (43), (44) and (45) as functions of α and β. The plots are shown starting from a minimum value (left to right) of $\alpha_{\min} = 0.1, 0.5, 1$ up to a maximum value of $\alpha_{\max} = 6$.

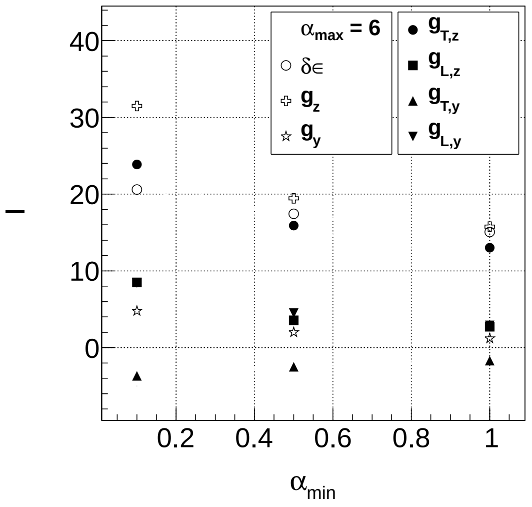

FIG. 5: Integrals of the functions $I_{g_{Tz}}, I_{g_{Ty}}, I_{g_{Lz}}, I_{g_{Ly}}$ and $I_{g_{\delta\epsilon}}$ over the domain $\alpha_{\rm min} < \alpha < \alpha_{\rm max}$, $-5 < \beta < 5$ for the different values of $\alpha_{\rm min}$. We also plot the values of the combinations $I_z \equiv I_{g_{Tz}} + I_{g_{Lz}}$ and $I_y \equiv I_{g_{Ty}} + I_{g_{Ly}}$. Notice that for all of values of $\alpha_{\rm min}$, the largest contribution to I_z comes from $I_{g_{Tz}}$, that is the wake or transverse mode whereas the largest contribution to I_y comes from $I_{g_{Ly}}$, that is the sound or longitudinal mode. Moreover, I_z is always larger than I_y.

result reads as

$$
\begin{aligned}
(\mathbf{g}_L)_z &= \left(\frac{\gamma}{4\pi}\right)\left(\frac{dE}{dx}\right)\left(\frac{2v}{3\Gamma_s}\right)^2 \left[\frac{\alpha}{(\alpha^2+\beta^2)^{\frac{3}{2}}}\right. \\
&- \frac{9}{16}\int_0^\infty ds \mathrm{J}_0\left(\frac{3}{4}\beta\sqrt{s(s+2)}\right) e^{-\frac{3}{4}\alpha s}\, (s \\
&+ \left.\left. c_s^2/v^2\left(\frac{3\alpha s}{2(s+1)} - \frac{2}{(s+1)^2} - 2\right)\right)\right] \\
&\equiv \left(\frac{\gamma}{4\pi}\right)\left(\frac{dE}{dx}\right)\left(\frac{2v}{3\Gamma_s}\right)^2 I_{g_{Lz}}(\alpha,\beta). \qquad (43)
\end{aligned}
$$

In a similar fashion we obtain

$$
\begin{aligned}
(\mathbf{g}_L)_y &= \left(\frac{\gamma}{4\pi}\right)\left(\frac{dE}{dx}\right)\left(\frac{2v}{3\Gamma_s}\right)^2 \left[\frac{\beta}{(\alpha^2+\beta^2)^{\frac{3}{2}}}\right. \\
&+ \frac{9}{16}\int_0^\infty ds \mathrm{J}_1\left(\frac{3}{4}\beta\sqrt{s(s+2)}\right) e^{-\frac{3}{4}\alpha s}\, (-1 \\
&+ \left.\left. c_s^2/v^2\left(\frac{2}{(s+1)^2} - \frac{3\alpha}{2(s+1)} - \frac{2}{s}\right)\right)\right] \\
&\equiv \left(\frac{\gamma}{4\pi}\right)\left(\frac{dE}{dx}\right)\left(\frac{2v}{3\Gamma_s}\right)^2 I_{g_{Ly}}(\alpha,\beta), \qquad (44)
\end{aligned}
$$

and

$$
\begin{aligned}
\delta\epsilon &= \left(\frac{\gamma}{4\pi}\right)\left(\frac{dE}{dx}\right)\left(\frac{2v}{3\Gamma_s}\right)^2\left(\frac{9}{8v}\right) \\
&\times \int_0^\infty ds \mathrm{J}_0\left(\frac{3}{4}\beta\sqrt{s(s+2)}\right) e^{-\frac{3}{4}\alpha s} \\
&\times \left[1 + \frac{2c_s^2/v^2}{s}\left(-1 + \frac{1+s\left(3+s+\frac{3}{4}\alpha(s+1)\right)}{(s+1)^2}\right)\right] \\
&\equiv \left(\frac{\gamma}{4\pi}\right)\left(\frac{dE}{dx}\right)\left(\frac{2v}{3\Gamma_s}\right)^2\left(\frac{9}{8v}\right) I_{\delta\epsilon}(\alpha,\beta). \qquad (45)
\end{aligned}
$$

Figure 4 shows three dimensional plots of $I_{g_{Tz}}, I_{g_{Ty}}, I_{g_{Lz}}, I_{g_{Ly}}$ and $I_{g_{\delta\epsilon}}$ as functions of α and β. Shown are also the corresponding contour plots. To test the sensitivity of the results on the distance to the source, the plots are shown starting from a minimum value of $\alpha_{\rm min} = 0.1, 0.5, 1$ up to a maximum value of $\alpha_{\rm max} = 6$. Figure 5 shows the integrals of the above functions over the domain $\alpha_{\rm min} < \alpha < \alpha_{\rm max}$, $-5 < \beta < 5$ for the different values of $\alpha_{\rm min}$. Shown also are the values of the combinations $I_z \equiv I_{g_{Tz}} + I_{g_{Lz}}$ and $I_y \equiv I_{g_{Ty}} + I_{g_{Ly}}$. Notice that for all of the shown values of $\alpha_{\rm min}$, the largest contribution to I_z comes from $I_{g_{Tz}}$, that is the wake or transverse mode whereas the largest contribution to I_y comes from $I_{g_{Ly}}$, that is the sound or longitudinal mode. Moreover, I_z is always larger than I_y. This last result shows that for the case treated here, where $c_s^2/v^2 < 1$, the momentum deposition will be preferentially forward peaked.

IV. AZIMUTHAL CORRELATIONS

We now proceed to use the formalism developed above to compute the azimuthal angular correlations for events where the leading hadron has a larger or equal momentum than the associated ones. Figure 6 shows the per-trigger correlations for the cases where the leading hadron is produced in a momentum range 3 GeV $\leq p_T \leq$ 4 GeV and the associated ones in the momentum ranges 0.4 GeV $\leq p_T \leq$ 1 GeV, 1 GeV $\leq p_T \leq$ 2 GeV, 2 GeV $\leq p_T \leq$ 3 GeV and 3 GeV $\leq p_T \leq$ 4 GeV, compared to data from PHENIX [2]. To obtain these correlations we have generated $2 \rightarrow 3$ hard scattering parton events using the MadGraph5 event generator [17], within the momentum window 10 GeV $\leq p_T \leq$ 12 GeV. Out of the three partons, we choose the one with the largest momentum to become the leading hadron by collinear fragmentation using the KKP parton fragmentation functions [18]. The other two partons in the event travel within the medium and thus represent the sources of energy-momentum deposition in the away-side. We consider that these partons travel 6 fm on average [12], and a medium induced energy loss per unit length $dE/dx = 2$ GeV/fm. Therefore in average, these partons transfer all of their initial momentum to the medium. For these away-side partons,

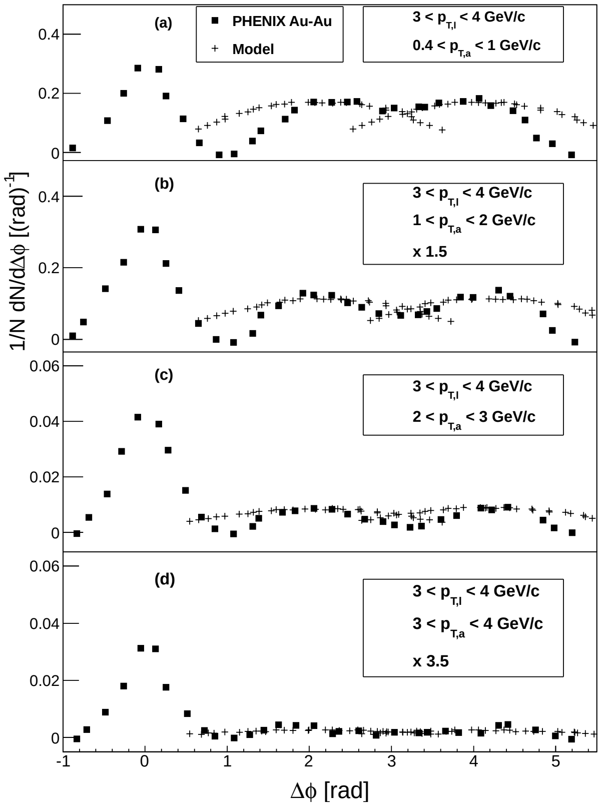

FIG. 6: Per-trigger azimuthal angular correlations. Shown are four different cases each one having the leading hadron produced with a fixed momentum range 3 GeV $\leq p_T \leq$ 4 GeV. From top to bottom the associated hadrons are in the momentum ranges 0.4 GeV $\leq p_T \leq$ 1 GeV, 1 GeV $\leq p_T \leq$ 2 GeV, 2 GeV $\leq p_T \leq$ 3 GeV and 3 GeV $\leq p_T \leq$ 4 GeV. The results are compared to data from PHENIX [2].

we compute the angular distribution around their direction of motion by means of the Cooper-Frye and linear viscous hydrodynamics formalisms, described in Secs. II and III. We use the value $\alpha_{\min} = 0.1$. Since we consider massless partons, we take their speed $v = 0.9995$c. The sound attenuation length is taken to be $\Gamma_s = 1/(3\pi T_0)$ which results from taking $\eta = 1/(4\pi)$ and consider the value T_0 =350 MeV, and the sound velocity $c_s = 1/\sqrt{3}$. In order to produce final state hadrons out of the away-side partons that emerge via the Cooper-Frye formula, we consider that the partons in the head shock region carry half of the hard scattering parton momentum. We subsequently let these partons produce final state hadrons using once again the KKP in vacuum fragmentation functions. This procedure is intended to mimic surface emission of the leading parton together with in-medium energy-momentum deposited by the away-side ones. The hadron momentum distributions obtained from the leading and associate partons are shown in Figs. 7 and 8, respectively.

Notice that Fig. 6 shows a quite good agreement of this simple scenario with the correlation data, particularly since it reproduces the systematics of double-hump decreasing intensity as the momentum of the away-side hadrons becomes closer to the momentum of the leading hadron.

V. SUMMARY AND CONCLUSIONS

In this work, we have studied the way that fast moving partons deposit their energy-momentum when traveling in a medium. We have shown that for conditions resembling a medium produced in a heavy ion reaction, energy-momentum is preferentially deposited along the head-shock and that in order to produce a double-hump structure in the away-side of azimuthal correlations, one can consider that two partons, instead of one, travel towards the away-side. We have argued that these away-side partons can be originally produced by a $2 \rightarrow 3$ hard scattering. Even though $2 \rightarrow 3$ parton processes are suppressed with respect to $2 \rightarrow 2$ ones by and extra power of α_s, there is also a kinematic enhancement that partially compensates. This is due to the fact that for a given energy deposited in the away-side, the partons from $2 \rightarrow 3$ processes are produced with lower momentum than the away-side parton in $2 \rightarrow 2$ processes, thus the former are more copiously produced.

We have resorted to linear viscous hydrodynamics to compute the medium response to the fast moving partons and the Cooper-Frye formula to compute the parton distribution originated from this disturbance in a static background medium. To mimic a scenario where

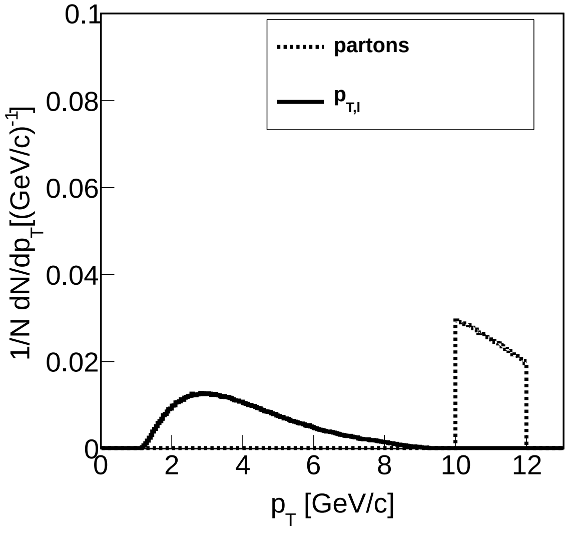

FIG. 7: Hadron momentum distribution obtained from a leading parton with momentum in the range 10 GeV $\leq p_T \leq$ 12 GeV.

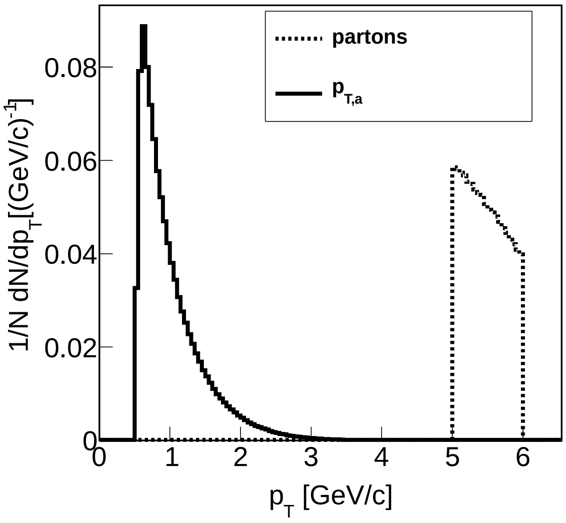

FIG. 8: Hadron momentum distribution obtained from an associated parton with momentum in the range 5 GeV $\leq p_T \leq$ 6 GeV.

the leading hadron comes from surface emission and the away-side partons deposit all of their original energy-momentum within the medium, we have selected partons produced in 2 → 3 processes, evolving the parton with the highest energy to become the leading hadron using KKP in vacuum fragmentation. Also, the head-shock region around the direction of motion of the away-side partons, is assumed to carry half of the original hard-scattering parton momentum. The partons in the head-shock region are then hadronized using also KKP in vacuum fragmentation. The comparison to PHENIX data shows that this simple scenario reproduces the systematics of a decreasing away-side correlation when the momentum of the associated hadrons becomes closer to the momentum of the leading hadron. This scenario seems to avoid the shortcomings of the Mach cone as the origin of the double-hump structure in the away-side. A more detailed analysis is currently under way to explore the systematics of away-side correlations for a larger set of conditions and will be reported elsewhere.

Acknowledgments

Support for this work has been received in part from DGAPA-UNAM under grant number PAPIIT-IN103811, CONACyT-México under grant number 128534 and *Programa de Intercambio UNAM-UNISON.*

[1] C. Adler *et al.* (STAR Collaboration), Phys. Rev. Lett. **90** 082302 (2003).

[2] A. Adate *et al.* (PHENIX Collaboration), Phys. Rev. C **78**, 014901 (2008).

[3] M. M. Aggarwal *et al.* (STAR Collaboration), Phys. Rev. C **82**, 024912 (2010); A. Adare *et al.* (PHENIX Collaboration), Phys. Rev. Lett. **104**, 252301 (2010).

[4] J. Casalderrey-Solana, J. Phys. G **34**, S345 (2007).

[5] T. Renk and J. Ruppert, Phys. Rev. C **76**, 014908 (2007).

[6] J. Casalderrey-Solana, E. V. Shuryak and D. Teaney, *Hydrodynamic flow from fast particles*, hep-ph/0602183.

[7] G. Torrieri, B. Betz, J. Noronha and M. Gyulassy, Acta Phys. Polon. **B39**, 3281 (2008).

[8] I. Bouras, A. El, O. Fochler, H. Niemi, Z. Xu and C. Greiner, Phys. Lett. B **710**, 641 (2012).

[9] R. B. Neufeld and I. Vitev, Phys. Rev. C **86**, 024905 (2012).

[10] P. Sorensen (STAR Collaboration), J. Phys. G **38**, 124029 (2011); K. Aamodt *et al.* (ALICE Collaboration), Phys. Rev. Lett. **107**, 032301 (2011).

[11] F. Wang (STAR Collaboration), arXiv:1201.5006; H. Agakishiev *et al.* (STAR Collaboration), arXiv:1010.0690.

[12] A. Ayala, J. Jalilian-Marian, J. Magnin, A. Ortiz, G. Paić and M. E. Tejeda-Yeomans, Phys. Rev. Lett. **104**, 042301 (2010); Phys. Rev. C **84**, 024915 (2011).

[13] A. Ayala, I. Dominguez, J. Jalilian-Marian, J. Magnin and M. E. Tejeda-Yeomans Phys. Rev. C **86**, 034901 (2012).

[14] F. Cooper and G. Frye, Phys. Rev. D **10**, 186 (1974).

[15] R. B. Neufeld, Phys. Rev. C **79**, 054909 (2009).

[16] R. B. Neufeld and T. Renk, Phys. Rev. C **82**, 044903 (2010).

[17] J. Alwall *et al.*, JHEP **1106**, 128 (2011).

[18] B.A. Kniehl, G. Kreimer and B. Potter, Nucl. Phys. B **582**, 514 (2000).